Archive of SID

Journal of Solid Mechanics Vol. 2, No. 2 (2010) pp. 115-128

Creep Stress Redistribution Analysis of Thick-Walled FGM Spheres

S.M.A. Aleayoub[1], A. Loghman[2,*]

[1]*Department of Mechanical Engineering, Arak Branch, Islamic Azad University, Arak, Iran*
[2]*Department of Mechanical Engineering, Faculty of Engineering, University of Kashan, Kashan, Iran*

Received 17 May 2010; accepted 18 July 2010

ABSTRACT
Time-dependent creep stress redistribution analysis of thick-walled FGM spheres subjected to an internal pressure and a uniform temperature field is investigated. The material creep and mechanical properties through the radial graded direction are assumed to obey the simple power-law variation throughout the thickness. Total strains are assumed to be the sum of elastic, thermal and creep strains. Creep strains are time temperature and stress dependent. Using equations of equilibrium, compatibility and stress-strain relations a differential equation, containing creep strains, for radial stress is obtained. Ignoring creep strains in this differential equation, a closed form solution for initial thermo-elastic stresses at zero time is presented. Initial thermo-elastic stresses are illustrated for different material properties. Using Prandtl-Reuss relation in conjunction with the above differential equation and the Norton's law for the material uni-axial creep constitutive model, radial and tangential creep stress rates are obtained. These creep stress rates are containing integrals of effective stress and are evaluated numerically. Creep stress rates are plotted against dimensionless radius for different material properties. Using creep stress rates, stress redistributions are calculated iteratively using thermo-elastic stresses as initial values for stress redistributions. It has been found that radial stress redistributions are not significant for different material properties. However, major redistributions occur for tangential and effective stresses.

© 2010 IAU, Arak Branch. All rights reserved.

Keywords: FGM Spheres; Thermo-elastic Creep; Stress Redistribution

1 INTRODUCTION

FUNCTIONALLY graded materials are used in modern technologies for structural components such as those used in nuclear, aircraft, space engineering and pressure vessels. Elastic, plastic and creep stress analysis of these components have attracted wide attention due to combining different material properties and loading conditions. Time-dependent creep stress and damage analysis of thick-walled spherical pressure vessels of constant material properties have been investigated by Loghman and Shokouhi [1]. They studied the creep stress and damage histories of thick-walled spheres using the material constant creep and creep rupture properties defined by the theta projection concept [2]. Loading conditions included an internal pressure and a thermal gradient. Although intensive investigation considering creep of thick-walled spheres and cylinders with constant material properties can be found in the existing references- Loghman and Wahab [3], Sim and Penny [4]- little publication can be found dealing with time-dependent creep of FGM spheres and cylinders. Yang [5] presented a solution for time-dependent creep behavior of FGM cylinders. Following Norton's law for material creep behavior and using equations of equilibrium, strain displacement and stress strain relations and considering Prandtl-Reuss relations for creep strain rate-stress equation, he obtained a differential equation for the displacement rate. There was no exact solution of the equation.

* Corresponding author. Tel.: +98 361 591 2425; fax: +98 361 555 9930.
E-mail address: aloghman@kashanu.ac.ir (A. Loghman).

© 2010 IAU, Arak Branch. All rights reserved.

www.SID.ir

Archive of SID

With some simplifications and using Taylor expansion series, however, he obtained the displacement rate and then the stress rates were calculated. When the stress rates were known, the stresses at any time were calculated iteratively. Creep deformation and stresses in thick-walled cylindrical vessels of FGM subjected to internal pressure were presented by You et.al. [6]. They obtained a closed form solution for steady state creep stresses in FGM cylinders. Thermal stresses were not considered and stress redistributions were not presented. Time-dependent deformation and fracture of multi-material systems at high temperature were presented by Xuan et. al. [7]. They considered a thick-walled sphere of FGM material subjected to an internal pressure. Using Norton's law for material creep behavior and using equations of equilibrium, compatibility, stress-strain relations and considering the Prandtl-Reuss relations, obtained a differential equation for the radial stress rate. Radial and circumferential stress distributions with different material creep properties after two hundred hours were illustrated. In this work, however, thermal stresses are not included and stress redistributions are not considered.

The main objective of this paper is to present a time-dependent creep stress redistribution analysis of FGM spheres.

2 THEORETICAL ANALYSIS

2.1 Basic formulation for thermo elastic creep stress analysis of FGM spheres

Consider a sphere with an inner radius r_i and outer radius r_0 subjected to an internal pressure p and a uniform temperature field T. The total strains are the sum of elastic, thermal and creep strains

$$\varepsilon_r = c_{11}\sigma_r + 2c_{12}\sigma_\theta + \alpha_r T + \varepsilon_r^c \tag{1a}$$

$$\varepsilon_\theta = c_{12}\sigma_r + (c_{11}+c_{12})\sigma_\theta + \alpha_\theta T + \varepsilon_\theta^c \tag{1b}$$

where $c_{11} = 1/E$, $c_{12} = -\upsilon/E$ and α_r, α_θ are elastic and thermal expansion radial dependent coefficients respectively.

In this study, υ is considered to be a constant, E, α_r and α_θ are assumed to obey the power-law variation as $E = E_0 r^\varphi$ and $\alpha_r = \alpha_\theta = \alpha_0 r^\beta$.

The equilibrium and compatibility equations in spherical symmetry are written as

$$\frac{\mathrm{d}\sigma_r}{\mathrm{d}r} + \frac{2(\sigma_r - \sigma_\theta)}{r} = 0 \tag{2a}$$

$$\frac{\mathrm{d}\varepsilon_\theta}{\mathrm{d}r} + \frac{\varepsilon_\theta - \varepsilon_r}{r} = 0 \tag{2b}$$

Substituting the radial and circumferential strains from Eqs. (1a) and (1b) into the compatibility Eq. (2b) and using equilibrium Eq. (2a) the following differential equation for the radial stress is obtained

$$r^2\frac{\mathrm{d}^2\sigma_r}{\mathrm{d}r^2} + r(4-\varphi)\frac{\mathrm{d}\sigma_r}{\mathrm{d}r} - \frac{2\varphi(1-2\upsilon)}{(1-\upsilon)}\sigma_r = -\frac{2\alpha_0 E_0 \beta r^{(\varphi+\beta)}}{1-\upsilon}T - \frac{2E_0 r^{\varphi+1}}{1-\upsilon}\frac{\mathrm{d}\varepsilon_\theta^c}{\mathrm{d}r} - \frac{2E_0 r^\varphi}{1-\upsilon}(\varepsilon_\theta^c - \varepsilon_r^c) \tag{3}$$

where creep strains, ε_r^c and ε_θ^c on the right hand side of the above differential equation are time, temperature and stress dependent.

2.2 Thermoelastic stress analysis of FGM spheres

Ignoring the creep strain terms on the right hand side of the above differential equation gives the following differential equation for thermoelastic stress analysis

$$r^2\frac{\mathrm{d}^2\sigma_r}{\mathrm{d}r^2} + (4-\varphi)r\frac{\mathrm{d}\sigma_r}{\mathrm{d}r} - 2\varphi\upsilon'\sigma_r = Jr^{\varphi+\beta}T \tag{4}$$

www.SID.ir
© 2010 IAU, Arak Branch

Archive of SID

where

$$\upsilon' = \frac{1-2\upsilon}{1-\upsilon},\quad J = -\frac{2\alpha_0 E_0 \beta}{1-\upsilon} \tag{5}$$

It is obvious that the homogeneous solution to Eq. (4) can be obtained by assuming

$$\sigma_r = Cr^{\lambda} \tag{6}$$

Substituting Eq. (6) into Eq. (4) one can obtain the following characteristic equation

$$\lambda^2 + (3-\varphi)\lambda - 2\varphi\upsilon' = 0 \tag{7}$$

The roots of Eq. (7) are

$$\lambda_1 = \frac{\varphi-3}{2} + \frac{1}{2}\sqrt{(3-\varphi)^2 + 8\varphi\upsilon'} \tag{8a}$$

$$\lambda_2 = \frac{\varphi-3}{2} - \frac{1}{2}\sqrt{(3-\varphi)^2 + 8\varphi\upsilon'} \tag{8b}$$

Since $0.5 > \upsilon > 0$ the discriminant of Eq. (7) is always greater than zero. Therefore, λ_1 and λ_2 are real and distinct. The homogeneous solution of Eq. (4) is therefore

$$\sigma_{rh} = C_1 r^{\lambda_1} + C_2 r^{\lambda_2} \tag{9}$$

The particular solution of the differential Eq. (4) may be obtained as

$$\sigma_{rp} = u_1 r^{\lambda_1} + u_2 r^{\lambda_2} \tag{10}$$

where

$$u_1 = \int \frac{-r^{\lambda_2} R(r)}{W(r^{\lambda_1}, r^{\lambda_2})}\,\mathrm{d}r \tag{11}$$

$$u_1 = \int \frac{r^{\lambda_1} R(r)}{W(r^{\lambda_1}, r^{\lambda_2})}\,\mathrm{d}r \tag{12}$$

in which $R(r) = Jr^{\varphi+\beta}T$ is the expression on the right hand side of Eq.(4) and W is defined as

$$W(r^{\lambda_1}, r^{\lambda_2}) = \begin{vmatrix} r^{\lambda_1} & r^{\lambda_2} \\ \lambda_1 r^{\lambda_1 - 1} & \lambda_2 r^{\lambda 2 - 1} \end{vmatrix} = (\lambda_2 - \lambda_1) r^{\lambda_2 + \lambda_1 - 1} \tag{13}$$

Therefore, u_1 and u_2 may be obtained by the following integration

$$u_1 = \int \frac{r^{\lambda_2}\,\dfrac{2E_0\alpha_0\beta T}{1-\upsilon} r^{\beta+\varphi}}{(\lambda_2 - \lambda_1) r^{\lambda_2+\lambda_1-1}}\,\mathrm{d}r = \frac{2E_0\alpha_0\beta T}{(1-\upsilon)(\lambda_2 - \lambda_1)(\beta+\varphi-\lambda_1+2)} r^{\beta+\varphi-\lambda_1+2} \tag{14}$$

$$u_2 = -\int \frac{r^{\lambda_1}\,\dfrac{2E_0\alpha_0\beta T}{1-\upsilon} r^{\beta+\varphi}}{(\lambda_2 - \lambda_1) r^{\lambda_2+\lambda_1-1}}\,\mathrm{d}r = -\frac{2E_0\alpha_0\beta T}{(1-\upsilon)(\lambda_2 - \lambda_1)(\beta+\varphi-\lambda_2+2)} r^{\beta+\varphi-\lambda_2+2} \tag{15}$$

www.SID.ir
© 2010 IAU, Arak Branch

Archive of SID

Substituting Eqs. (14) and (15) into Eq. (10) one can obtain the particular solution

$$\sigma_{rp} = -\frac{2E_0\alpha_0\beta T}{(1-\upsilon)(\beta+\varphi-\lambda_1+2)(\beta+\varphi-\lambda_2+2)} r^{\beta+\varphi+2} \tag{16}$$

The complete solution of Eq. (4) can be written as

$$\sigma_r = C_1 r^{\lambda_1} + C_2 r^{\lambda_2} - G r^{\beta+\varphi+2} \tag{17}$$

where

$$G = \frac{2E_0\alpha_0\beta T}{(1-\upsilon)(\beta+\varphi-\lambda_1+2)(\beta+\varphi-\lambda_2+2)} \tag{18}$$

Using Eq. (2a) the expression for the tangential stress may be written as

$$\sigma_\theta = (1+\frac{\lambda_1}{2})C_1 r^{\lambda_1} + (1+\frac{\lambda_2}{2})C_2 r^{\lambda_2} - (1+\frac{\beta+\varphi+2}{2})G r^{\beta+\varphi+2} \tag{19}$$

The constants C_1 and C_2 are determined from the boundary conditions

$$\begin{aligned} &\text{at } r = r_i \rightarrow \sigma_r = -p \\ &\text{at } r = r_0 \rightarrow \sigma_r = 0 \end{aligned} \tag{20}$$

Substituting the above boundary condition into Eq. (17) the constants C_1 and C_2 are obtained

$$C_1 = \frac{G(r_0^{\beta+\varphi+2} r_i^{\lambda_2} - r_i^{\beta+\varphi+2} r_0^{\lambda_2}) + p r_0^{\lambda_2}}{r_i^{\lambda_2} r_0^{\lambda_1} - r_i^{\lambda_1} r_0^{\lambda_2}} \tag{21a}$$

$$C_2 = \frac{G(r_i^{\beta+\varphi+2} r_0^{\lambda_1} - r_0^{\beta+\varphi+2} r_i^{\lambda_1}) - p r_0^{\lambda_1}}{r_i^{\lambda_2} r_0^{\lambda_1} - r_i^{\lambda_1} r_0^{\lambda_2}} \tag{21b}$$

Substituting the constants C_1 and C_2 from Eqs. (21a) and (21b) into Eqs. (17) and (19) and using Eq. (18) the expressions for radial and circumferential thermoelastic stresses are obtained

$$\begin{aligned} \sigma_r = {} & \frac{2E_0\alpha_0\beta T}{(1-\upsilon)(\beta+\varphi-\lambda_1+2)(\beta+\varphi-\lambda_2+2)} \{ [\frac{(r_0^{\beta+\varphi+2} r_i^{\lambda_2} - r_i^{\beta+\varphi+2} r_0^{\lambda_2})}{r_i^{\lambda_2} r_0^{\lambda_1} - r_i^{\lambda_1} r_0^{\lambda_2}}] r^{\lambda_1} \\ & + [\frac{(r_i^{\beta+\varphi+2} r_0^{\lambda_1} - r_0^{\beta+\varphi+2} r_i^{\lambda_1})}{r_i^{\lambda_2} r_0^{\lambda_1} - r_i^{\lambda_1} r_0^{\lambda_2}}] r^{\lambda_2} - r^{\beta+\varphi+2} \} + \frac{p(r_0^{\lambda_2} r^{\lambda_1} - r_0^{\lambda_1} r^{\lambda_2})}{r_i^{\lambda_2} r_0^{\lambda_1} - r_i^{\lambda_1} r_0^{\lambda_2}} \end{aligned} \tag{22a}$$

$$\begin{aligned} \sigma_\theta = {} & \frac{2E_0\alpha_0\beta T}{(1-\upsilon)(\beta+\varphi-\lambda_1+2)(\beta+\varphi-\lambda_2+2)} \{ (1+\frac{\lambda_1}{2}) [\frac{(r_0^{\beta+\varphi+2} r_i^{\lambda_2} - r_i^{\beta+\varphi+2} r_0^{\lambda_2})}{r_i^{\lambda_2} r_0^{\lambda_1} - r_i^{\lambda_1} r_0^{\lambda_2}}] r^{\lambda_1} \\ & + (1+\frac{\lambda_2}{2}) [\frac{(r_i^{\beta+\varphi+2} r_0^{\lambda_1} - r_0^{\beta+\varphi+2} r_i^{\lambda_1})}{r_i^{\lambda_2} r_0^{\lambda_1} - r_i^{\lambda_1} r_0^{\lambda_2}}] r^{\lambda_2} - (1+\frac{\beta+\varphi+2}{2}) r^{\beta+\varphi+2} \} \\ & + \frac{p[(1+\frac{\lambda_1}{2}) r_0^{\lambda_2} r^{\lambda_1} - (1+\frac{\lambda_2}{2}) r_0^{\lambda_1} r^{\lambda_2})]}{r_i^{\lambda_2} r_0^{\lambda_1} - r_i^{\lambda_1} r_0^{\lambda_2}} \end{aligned} \tag{22b}$$

www.SID.ir
© 2010 IAU, Arak Branch

Archive of SID

The above thermoelastic stresses are the initial elastic stress distribution which will be changed with time as the creep process progresses. These thermoelastic stresses and the effective stresses are shown in Figs. 1-3 for different material properties.

2.3 Time-dependent creep stress analysis of FGM spheres

Considering the temperature field to be steady, the differential equation (3) containing creep strains may be rewritten in terms of creep strain rates as follows

$$r^2\frac{\mathrm{d}^2\dot{\sigma}_r}{\mathrm{d}r^2}+r(4-\varphi)\frac{\mathrm{d}\dot{\sigma}_r}{\mathrm{d}r}-\frac{2\varphi(1-2\upsilon)}{(1-\upsilon)}\dot{\sigma}_r=-\frac{2E_0r^{\varphi+1}}{1-\upsilon}\frac{\mathrm{d}\dot{\varepsilon}_\theta^c}{\mathrm{d}r}-\frac{2E_0r^{\varphi}}{1-\upsilon}(\dot{\varepsilon}_\theta^c-\dot{\varepsilon}_r^c) \tag{23}$$

The creep strain rates are related to the current stresses and the material uniaxial creep constitutive model by the well-known Prandtl-Reuss equation

$$\dot{\varepsilon}_r^c=\frac{\dot{\varepsilon}_e}{\sigma_e}\left[\sigma_r-\sigma_\theta\right] \tag{24a}$$

$$\dot{\varepsilon}_\theta^c=\frac{\dot{\varepsilon}_e}{2\sigma_e}[\sigma_\theta-\sigma_r] \tag{24b}$$

in which the material uniaxial creep constitutive model is defined by the Norton's equation

$$\dot{\varepsilon}_e=B(r)\sigma_e^{n(r)} \tag{25}$$

where $B(r)=b_0r^{b_1}$ and $n(r)$ is considered to be a constant $n(r)=n_0$ in this study. Substituting from Eq. (25) into Eqs. (24a) and (24b) one can obtain

$$\dot{\varepsilon}_r^c=B(r)\sigma_e^{n-1}[\sigma_r-\sigma_\theta] \tag{26a}$$

$$\dot{\varepsilon}_\theta^c=\frac{B(r)\sigma_e^{n-1}}{2}[\sigma_\theta-\sigma_r] \tag{26b}$$

The Von-Mises and Tresca's equivalent stress are the same in spherical symmetry

$$\sigma_e=\left|\sigma_\theta-\sigma_r\right| \tag{27}$$

In the absence of temperature field, tangential stress is always greater than radial stress. For many applicable loading combinations, however, tangential stress is greater than radial stress. Therefore, Eqs. (26a) and (26b) may be written as follows

$$\dot{\varepsilon}_r^c=-B(r)\sigma_e^n \tag{28a}$$

$$\dot{\varepsilon}_\theta^c=\frac{B(r)\sigma_e^n}{2} \tag{28b}$$

Substituting from Eqs. (28a) and (28b) into differential Eq. (23) the following differential equation is obtained

$$r^2\frac{\mathrm{d}^2\dot{\sigma}_r}{\mathrm{d}r^2}+r(4-\varphi)\frac{\mathrm{d}\dot{\sigma}_r}{\mathrm{d}r}-\frac{2\varphi(1-2\upsilon)}{(1-\upsilon)}\dot{\sigma}_r=-\frac{E_0r^{\varphi+1}}{1-\upsilon}\{[\frac{\mathrm{d}}{\mathrm{d}r}+\frac{3}{r}](B(r)\sigma_e^n)\} \tag{29}$$

The homogeneous solution of this differential equation is therefore

www.SID.ir
© 2010 IAU, Arak Branch

Archive of SID

$$\dot{\sigma}_{rh} = D_1 r^{\lambda_1} + D_2 r^{\lambda_2} \tag{30}$$

where λ_1 and λ_2 are defined in Eqs. (8a) and (8b). The particular solution can be obtained similar to thermo-elastic solution as

$$u_1 = \int \frac{r^{\lambda_2} \dfrac{rE}{1-\upsilon}\{[\dfrac{d}{dr}+\dfrac{3}{r}](B(r)\sigma_e^n)\}}{(\lambda_2-\lambda_1)r^{\lambda_2+\lambda_1-1}}\,\mathrm{d}r \tag{31}$$

$$u_2 = -\int \frac{r^{\lambda_1} \dfrac{rE}{1-\upsilon}\{[\dfrac{d}{dr}+\dfrac{3}{r}](B(r)\sigma_e^n)\}}{(\lambda_2-\lambda_1)r^{\lambda_2+\lambda_1-1}}\,\mathrm{d}r \tag{32}$$

Eqs. (31) and (32) may be written

$$u_1 = \frac{E_0}{(1-\upsilon)(\lambda_2-\lambda_1)}[\int r^{2+\varphi-\lambda_2}\frac{d}{dr}(B\sigma_e^n)\,\mathrm{d}r + 3\int r^{1+\varphi-\lambda_2}\frac{d}{dr}(B\sigma_e^n)\,\mathrm{d}r] \tag{33}$$

$$u_2 = -\frac{E_0}{(1-\upsilon)(\lambda_2-\lambda_1)}[\int r^{2+\varphi-\lambda_2}\frac{d}{dr}(B\sigma_e^n)\,\mathrm{d}r + 3\int r^{1+\varphi-\lambda_2}\frac{d}{dr}(B\sigma_e^n)\,\mathrm{d}r] \tag{34}$$

Selecting $u = r^{2+\varphi-\lambda_2}$ and $\mathrm{d}v = \dfrac{\mathrm{d}}{\mathrm{d}r}(B\sigma_e^n)\,\mathrm{d}r$ and using $(\int u\,\mathrm{d}v = u.v - \int v\,\mathrm{d}u)$ integration by part one can obtain

$$u_1 = \frac{E_0}{(1-\upsilon)(\lambda_2-\lambda_1)}[r^{2+\varphi-\lambda_2}(B\sigma_e^n) + (1-\varphi+\lambda_1)\int r^{1+\varphi-\lambda_2}(B\sigma_e^n)\,\mathrm{d}r] \tag{35}$$

$$u_2 = -\frac{E_0}{(1-\upsilon)(\lambda_2-\lambda_1)}[r^{2+\varphi-\lambda_2}(B\sigma_e^n) + (1-\varphi+\lambda_2)\int r^{1+\varphi-\lambda_2}(B\sigma_e^n)\,\mathrm{d}r] \tag{36}$$

Then, the particular solution may be written as

$$\dot{\sigma}_{rp} = u_1 r^{\lambda_1} + u_2 r^{\lambda_2} \tag{37}$$

The general solution for the radial stress rate may be written

$$\dot{\sigma}_r = D_1 r^{\lambda_1} + D_2 r^{\lambda_2} + u_1 r^{\lambda_1} + u_2 r^{\lambda_2} \tag{38}$$

Substituting from Eqs. (35) and (36) into Eq. (38) one can get the radial stress rate and then the tangential stress rate as

$$\begin{aligned}\dot{\sigma}_r = {} & D_1 r^{\lambda_1} + D_2 r^{\lambda_2} + \frac{E_0}{(1-\upsilon)(\lambda_2-\lambda_1)}[(1-\varphi+\lambda_1)r^{\lambda_1}\int r^{1+\varphi-\lambda_1}(B\sigma_e^n)\,\mathrm{d}r \\ & -(1-\varphi+\lambda_2)r^{\lambda_2}\int r^{1+\varphi-\lambda_2}(B\sigma_e^n)\,\mathrm{d}r]\end{aligned} \tag{39}$$

$$\begin{aligned}\dot{\sigma}_\theta = {} & (\frac{\lambda_1}{2}+1)r^{\lambda_1}[D_1 + \frac{E_0}{(1-\upsilon)(\lambda_2-\lambda_1)}(1-\varphi+\lambda_1)\int r^{1+\varphi-\lambda_1}(B\sigma_e^n)\,\mathrm{d}r] \\ & +(\frac{\lambda_2}{2}+1)r^{\lambda_2}[D_2 - \frac{E_0}{(1-\upsilon)(\lambda_2-\lambda_1)}[(1-\varphi+\lambda_2)\int r^{1+\varphi-\lambda_2}(B\sigma_e^n)\,\mathrm{d}r] - \frac{E_0}{2(1-\upsilon)}r^{2+\varphi}B\sigma_e^n\end{aligned} \tag{40}$$

www.SID.ir
© 2010 IAU, Arak Branch

Archive of SID

Since inside and outside pressures do not change with time, the boundary conditions for stress rates at the inner and outer surfaces may be written

$$\text{at } r = r_i \rightarrow \dot{\sigma}_r = 0 \tag{41a}$$

$$\text{at } r = r_0 \rightarrow \dot{\sigma}_r = 0 \tag{41b}$$

Using the above boundary conditions, the constants D_1 and D_2 are obtained

$$\begin{aligned} D_1 = {} & \frac{E_0}{(1-\upsilon)(\lambda_2-\lambda_1)(1-(\frac{r_0}{r_i})^{\lambda_2-\lambda_1})}\{(1-\varphi+\lambda_1)[(\frac{r_0}{r_i})^{\lambda_2-\lambda_1}(\int r^{1+\varphi-\lambda_1}(B\sigma_e^n)\,\mathrm{d}r)_{r=r_i} \\ & -\int r^{1+\varphi-\lambda_1}(B\sigma_e^n)\,\mathrm{d}r)_{r=r_0}]-(1-\varphi+\lambda_2)r_0^{\lambda_2-\lambda_1}[(\int r^{1+\varphi-\lambda_2}(B\sigma_e^n)\,\mathrm{d}r)_{r=r_i}-\int r^{1+\varphi-\lambda_2}(B\sigma_e^n)\,\mathrm{d}r)_{r=r_0}]\} \end{aligned} \tag{42}$$

$$\begin{aligned} D_2 = {} & -\frac{E_0}{(1-\upsilon)(\lambda_2-\lambda_1)(1-(\frac{r_0}{r_i})^{\lambda_2-\lambda_1})}\{(1-\varphi+\lambda_1)r_i^{\lambda_1-\lambda_2}[(\int r^{1+\varphi-\lambda_1}(B\sigma_e^n)\,\mathrm{d}r)_{r=r_i} \\ & -\int r^{1+\varphi-\lambda_1}(B\sigma_e^n)\,\mathrm{d}r)_{r=r_0}]-(1-\varphi+\lambda_2)[(\int r^{1+\varphi-\lambda_2}(B\sigma_e^n)\,\mathrm{d}r)_{r=r_i}-(\frac{r_0}{r_i})^{\lambda_2-\lambda_1}(\int r^{1+\varphi-\lambda_2}(B\sigma_e^n)\,\mathrm{d}r)_{r=r_0}]\} \end{aligned} \tag{43}$$

Substituting from Eqs. (42) and (43) into Eqs. (39) and (40) the stress rates can be written as follows

$$\begin{aligned} \dot{\sigma}_r = {} & \frac{E_0}{(1-\upsilon)(\lambda_2-\lambda_1)(1-(\frac{r_0}{r_i})^{\lambda_2-\lambda_1})}\{(1-\varphi+\lambda_1)[(\frac{r_0}{r_i})^{\lambda_2-\lambda_1}(\int r^{1+\varphi-\lambda_1}(B\sigma_e^n)\,\mathrm{d}r)_{r=r_i} \\ & -\int r^{1+\varphi-\lambda_1}(B\sigma_e^n)\,\mathrm{d}r)_{r=r_0}]-(1-\varphi+\lambda_2)r_0^{\lambda_2-\lambda_1}[(\int r^{1+\varphi-\lambda_2}(B\sigma_e^n)\,\mathrm{d}r)_{r=r_i} \\ & -\int r^{1+\varphi-\lambda_2}(B\sigma_e^n)\,\mathrm{d}r)_{r=r_0}]\}r^{\lambda_1} \\ & -\frac{E_0}{(1-\upsilon)(\lambda_2-\lambda_1)(1-(\frac{r_0}{r_i})^{\lambda_2-\lambda_1})}\{(1-\varphi+\lambda_1)r_i^{\lambda_1-\lambda_2}[(\int r^{1+\varphi-\lambda_1}(B\sigma_e^n)\,\mathrm{d}r)_{r=r_i}-\int r^{1+\varphi-\lambda_1}(B\sigma_e^n)\,\mathrm{d}r)_{r=r_0} \\ & -(1-\varphi+\lambda_2)[(\int r^{1+\varphi-\lambda_2}(B\sigma_e^n)\,\mathrm{d}r)_{r=r_i}-(\frac{r_0}{r_i})^{\lambda_2-\lambda_1}(\int r^{1+\varphi-\lambda_2}(B\sigma_e^n)\,\mathrm{d}r)_{r=r_0}]\}r^{\lambda_2} \\ & +\frac{E_0}{(1-\upsilon)(\lambda_2-\lambda_1)}[(1-\varphi+\lambda_1)r^{\lambda_1}\int r^{1+\varphi-\lambda_1}(B\sigma_e^n)\,\mathrm{d}r-(1-\varphi+\lambda_2)r^{\lambda_2}\int r^{1+\varphi-\lambda_2}(B\sigma_e^n)\,\mathrm{d}r] \end{aligned} \tag{44}$$

$$\begin{aligned} \dot{\sigma}_\theta = {} & (\frac{\lambda_1}{2}+1)r^{\lambda_1}[\frac{E_0}{(1-\upsilon)(\lambda_2-\lambda_1)(1-(\frac{r_0}{r_i})^{\lambda_2-\lambda_1})}\{(1-\varphi+\lambda_1)[(\frac{r_0}{r_i})^{\lambda_2-\lambda_1}(\int r^{1+\varphi-\lambda_1}(B\sigma_e^n)dr)_{r=r_i} \\ & -\int r^{1+\varphi-\lambda_1}(B\sigma_e^n)dr)_{r=r_0}]-(1-\varphi+\lambda_2)r_0^{\lambda_2-\lambda_1}[(\int r^{1+\varphi-\lambda_2}(B\sigma_e^n)dr)_{r=r_i} \\ & -\int r^{1+\varphi-\lambda_2}(B\sigma_e^n)dr)_{r=r_0}]\}+\frac{E_0}{(1-\upsilon)(\lambda_2-\lambda_1)}(1-\varphi+\lambda_1)\int r^{1+\varphi-\lambda_1}(B\sigma_e^n)dr] \\ & +(\frac{\lambda_2}{2}+1)r^{\lambda_2}[-\frac{E_0}{(1-\upsilon)(\lambda_2-\lambda_1)(1-(\frac{r_0}{r_i})^{\lambda_2-\lambda_1})}\{(1-\varphi+\lambda_1)r_i^{\lambda_1-\lambda_2}[(\int r^{1+\varphi-\lambda_1}(B\sigma_e^n)dr)_{r=r_i} \\ & -\int r^{1+\varphi-\lambda_1}(B\sigma_e^n)dr)_{r=r_0}]-(1-\varphi+\lambda_2)[(\int r^{1+\varphi-\lambda_2}(B\sigma_e^n)dr)_{r=r_i} \end{aligned}$$

www.SID.ir

© 2010 IAU, Arak Branch

Archive of SID

$$-(\frac{r_0}{r_i})^{\lambda_2-\lambda_1}(\int r^{1+\varphi-\lambda_2}(B\sigma_e^n)dr)_{r=r_0}]\}-\frac{E_0}{(1-\upsilon)(\lambda_2-\lambda_1)}[(1-\varphi+\lambda_2)\int r^{1+\varphi-\lambda_2}(B\sigma_e^n)dr]$$
$$-\frac{E_0}{2(1-\upsilon)}r^{2+\varphi}B\sigma_e^n \tag{45}$$

Radial and tangential stress rates are obtained from Eqs. (43) and (44) and plotted against dimensionless radius for different material properties in Figs. 4 and 5. When the stress rates are known, time-dependent creep stress redistributions at any time t_i are obtained iteratively

$$\sigma_r^{(i)}(r,t_i)=\sigma_r^{(i-1)}(r,t_{i-1})+\dot{\sigma}_r^{(i)}(r,t_i)\ \mathrm{d}t^{(i)} \tag{46a}$$
$$\sigma_\theta^{(i)}(r,t_i)=\sigma_\theta^{(i-1)}(r,t_{i-1})+\dot{\sigma}_\theta^{(i)}(r,t_i)\ \mathrm{d}t^{(i)} \tag{46b}$$

where

$$t_i=\sum_{k=0}^{i}\mathrm{d}t^{(k)} \tag{47}$$

To calculate $\sigma_r^{(i)}(r,t_i)$ and $\sigma_\theta^{(i)}(r,t_i)$, the stresses at the time t_{i-1} are used. The solution at zero time $t_i=0$ corresponds to thermo-elastic stresses.

3 RESULTS AND DISCUSSION

The results presented here in this study are based on the following data for geometry, material properties, and loading conditions in a thick-walled FGM sphere

$r_o/r_i=1.2,\ E_o=22000$ MPa, $b_o=1.1\times10^{-30},\ b_1=-5,\ n_0=8,\ \upsilon=0.3,\ \alpha_o=1.2\times10^{-6}\ 1/^{\circ}\mathrm{C},$
$\beta=\varphi=2,1,-1,-2,\ T=200^{\circ}\mathrm{C},\ P_o=0,\ P_i=100$ MPa

Initial thermoelastic radial stresses at zero time are shown in Fig. 1. The boundary conditions for radial stresses at the inner and outer surfaces of the sphere are satisfied for all material properties. There are not significant differences among radial stresses for all material properties. Tangential thermo-elastic stresses at zero time are shown in Fig. 2 for different material properties. They are tensile throughout thickness. For $\beta=\varphi=-2$ and $\beta=\varphi=-1,$ however, they are highly tensile at the inner surface of the vessel where the radial stresses are highly compressive. It means the maximum shear stress which is $\tau_{\max}=(\sigma_\theta-\sigma_r)/2$ will be very high at the inner surface of the vessel and can cause yielding to occur. Also highly tensile tangential stresses at the inner surface of the sphere will also decrease the fatigue life of the vessel. Therefore in selection of material for such a vessel, the material identified by $\beta=\varphi=2$ is the best because of the best shear stress distribution throughout thickness. This can be well understood from Fig. 3 which shows the effective stress distribution throughout thickness for all four cases of material properties. Effective stresses are, indeed, twice as the maximum shear stresses $(\sigma_e=2\tau_{\max})$. Therefore, it is clear from Fig. 3, that the material with $\beta=\varphi=2$ has a uniform and best shear stress distribution throughout thickness. In Fig. 3, a reference stress has also been identified in which the effective stresses are identical for all material properties.

Radial and tangential stress rates are plotted against dimensionless radius for different material properties in Figs. 4 and 5. Fig. 4 shows that the radial stress rates are zero at the inner and outer surfaces of the sphere which satisfy the boundary conditions. The maximum rate of change of radial stresses belong to $\beta=\varphi=-2$ and then $\beta=\varphi=-1,\ \beta=\varphi=1$ and $\beta=\varphi=2,$ respectively. Therefore, minimum changes in radial stresses with time will take place for the material identified by $\beta=\varphi=2$ as will be explained next in radial stress redistributions.

www.SID.ir
© 2010 IAU, Arak Branch

Archive of SID

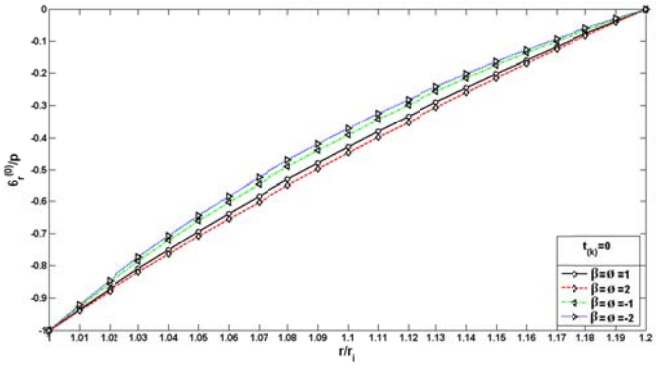

Fig. 1
Initial thermoelastic radial stresses in the FGM sphere for $\beta=\varphi=-2$, $\beta=\varphi=-1$, $\beta=\varphi=1$ and $\beta=\varphi=2$ at zero time.

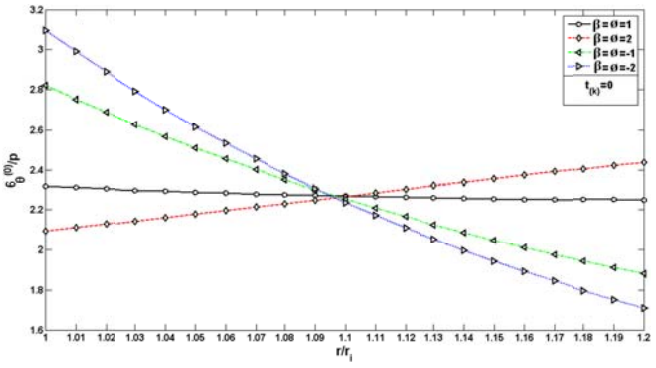

Fig. 2
Initial thermoelastic tangential stresses in the FGM sphere for $\beta=\varphi=-2$, $\beta=\varphi=-1$, $\beta=\varphi=1$ and $\beta=\varphi=2$ at zero time.

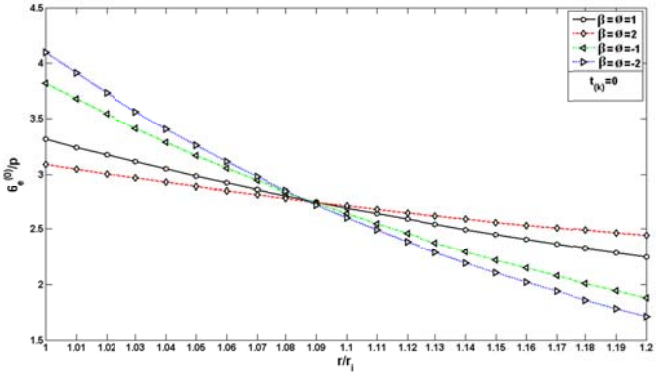

Fig. 3
Initial thermoelastic effective stresses in the FGM sphere for $\beta=\varphi=-2$, $\beta=\varphi=-1$, $\beta=\varphi=1$ and $\beta=\varphi=2$ at zero time.

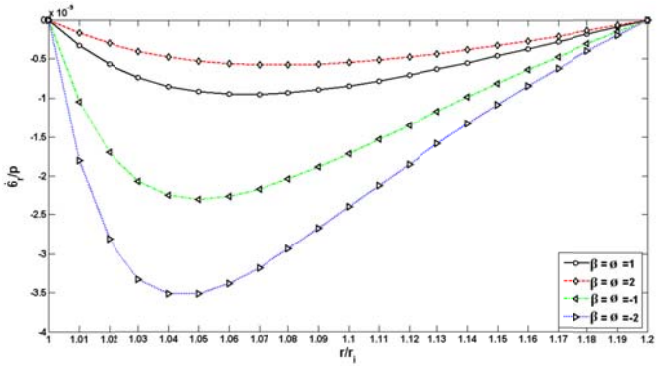

Fig. 4
Radial stress rates versus dimensionless radius in the FGM sphere for $\beta=\varphi=-2$, $\beta=\varphi=-1$, $\beta=\varphi=1$ and $\beta=\varphi=2$.

www.SID.ir

© 2010 IAU, Arak Branch

Archive of SID

Fig. 5 shows that the tangential stress rates are negative at almost a quarter part of the thickness located at the inside of the sphere and are positive at the remaining thickness of the vessel for all material properties. It means that the tangential stresses will be decreasing with time at the inner part of the vessel and will be increasing at the remaining part of the sphere. It is also clear from Fig. 5 that the maximum changes in tangential stresses with time will take place for material $\beta = \varphi = -2$ and minimum changes will occur for $\beta = \varphi = 2$. This will be later discussed in tangential stress redistributions. Time-dependent creep stress redistributions for different materials identified by $\beta = \varphi = 2$, $\beta = \varphi = 1$, $\beta = \varphi = -1$ and $\beta = \varphi = -2$ are shown in Figs. 6-17. Fig. 6 shows radial stress redistribution in a FGM sphere identified by material property $\beta = \varphi = 2$. As it is expected from our discussion on radial stress rates, minimum changes has occurred with time from its initial thermoelastic distribution to its final distribution at the third selected time step. It also satisfies the boundary conditions at the inner and outer surfaces of the sphere.

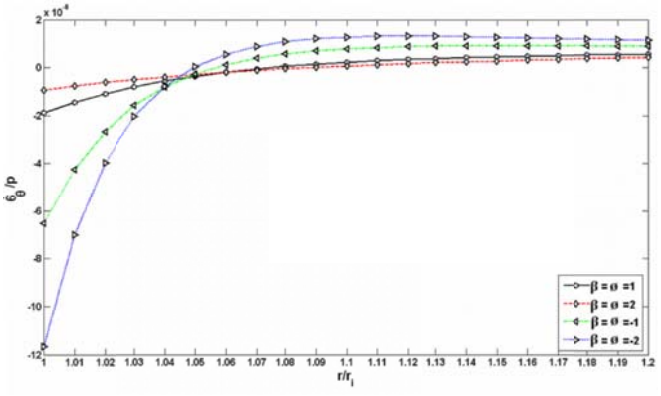

Fig. 5
Tangential stress rates versus dimensionless radius in the FGM sphere for $\beta = \varphi = -2$, $\beta = \varphi = -1$, $\beta = \varphi = 1$ and $\beta = \varphi = 2$.

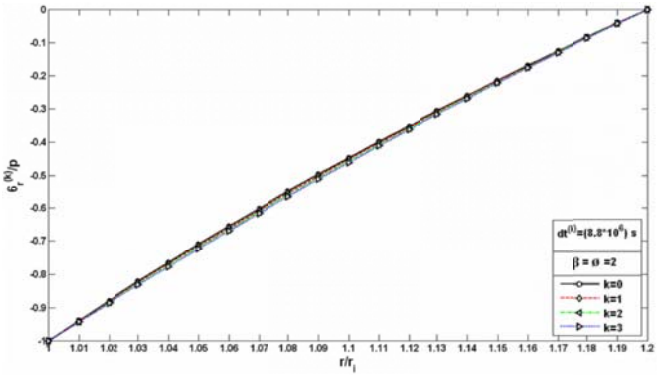

Fig. 6
Time-dependent radial creep stress redistribution in the FGM sphere from initial elastic at zero time to third selected time interval for the case $\beta = \varphi = 2$.

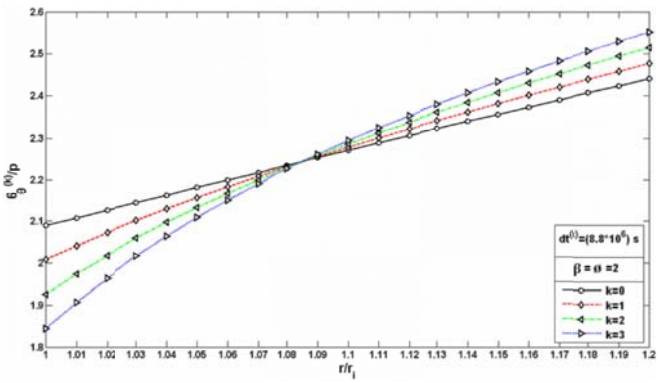

Fig. 7
Time-dependent tangential creep stress redistribution in the FGM sphere from initial elastic at zero time to third selected time interval for the case $\beta = \varphi = 2$.

www.SID.ir
© 2010 IAU, Arak Branch

Archive of SID

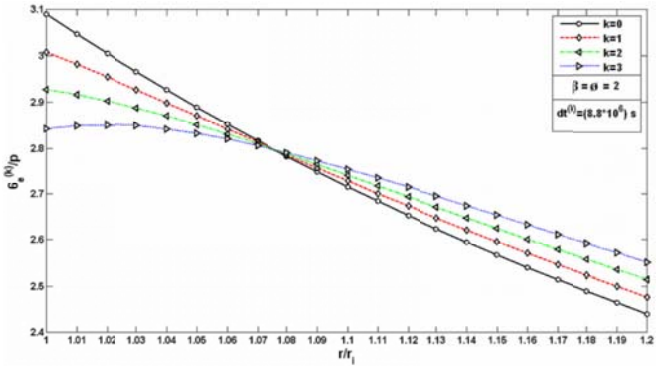

Fig. 8
Time-dependent effective creep stress redistribution in the FGM sphere from initial elastic at zero time to third selected time interval for the case $\beta = \varphi = 2$.

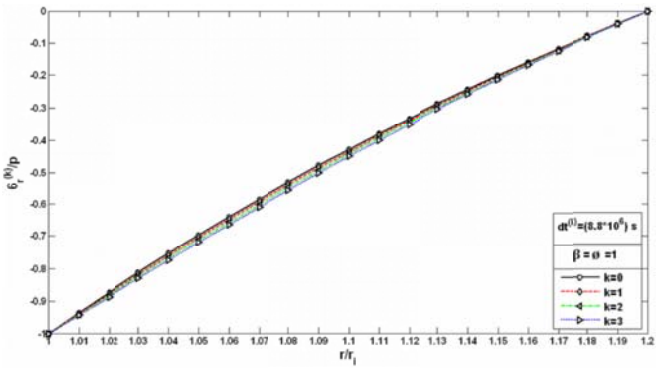

Fig. 9
Time-dependent radial creep stress redistribution in the FGM sphere from initial elastic at zero time to third selected time interval for the case $\beta = \varphi = 1$.

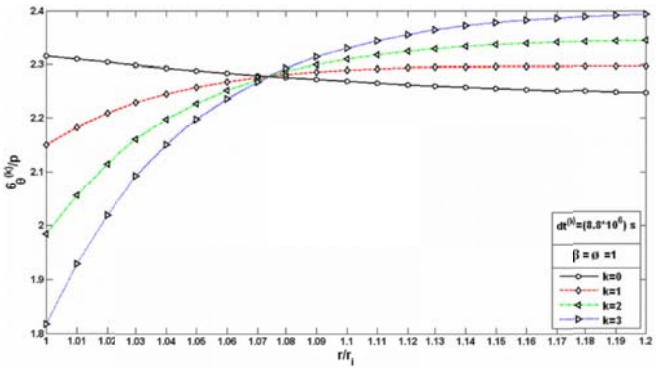

Fig. 10
Time-dependent tangential creep stress redistribution in the FGM sphere from initial elastic at zero time to third selected time interval for the case $\beta = \varphi = 1$.

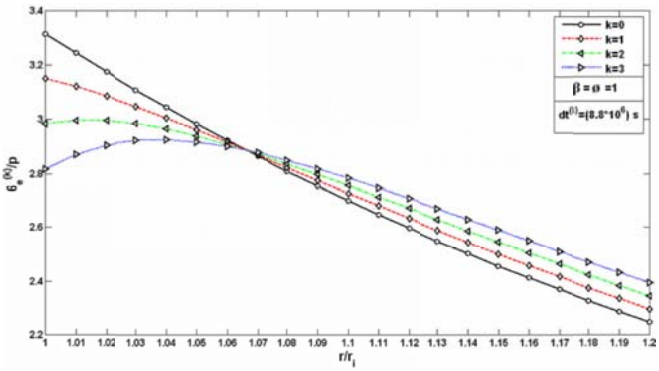

Fig. 11
Time-dependent effective creep stress redistribution in the FGM sphere from initial elastic at zero time to third selected time interval for the case $\beta = \varphi = 1$.

www.SID.ir

© 2010 IAU, Arak Branch

Archive of SID

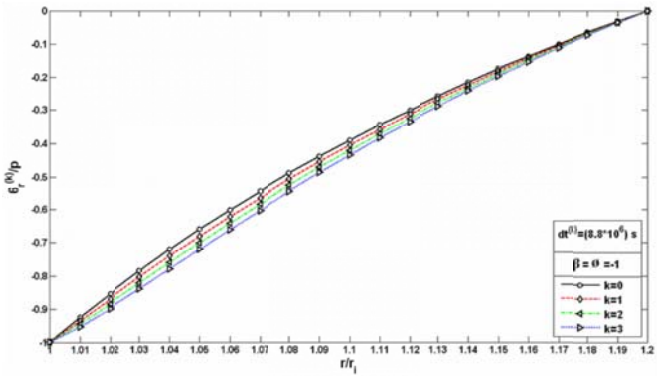

Fig. 12
Time-dependent radial creep stress redistribution in the FGM sphere from initial elastic at zero time to third selected time interval for the case $\beta=\varphi=-1$.

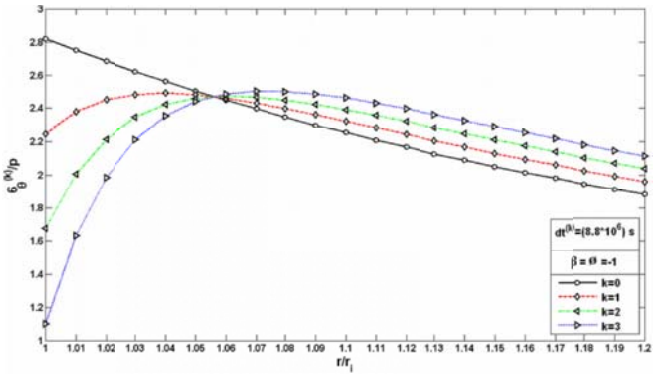

Fig. 13
Time-dependent tangential creep stress redistribution in the FGM sphere from initial elastic at zero time to third selected time interval for the case $\beta=\varphi=-1$.

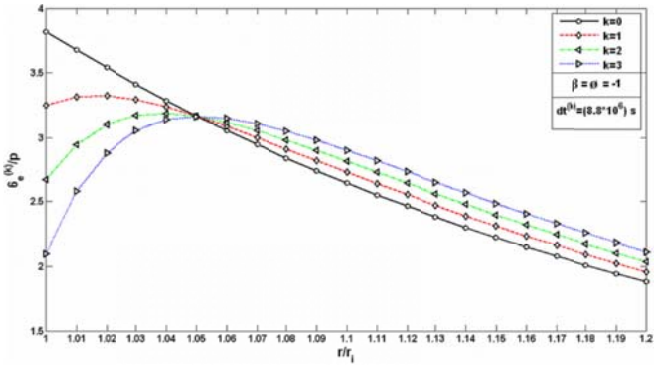

Fig. 14
Time-dependent effective creep stress redistribution in the FGM sphere from initial elastic at zero time to third selected time interval for the case $\beta=\varphi=-1$.

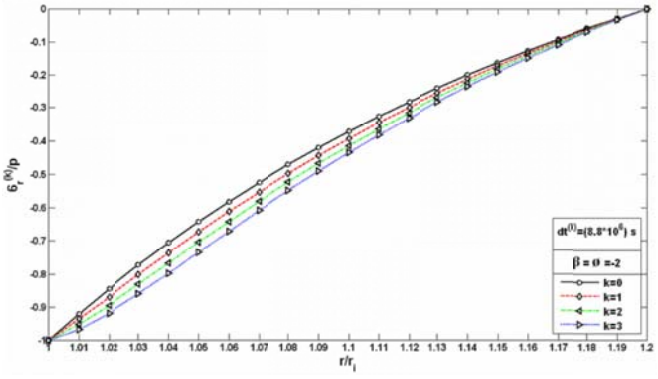

Fig. 15
Time-dependent radial creep stress redistribution in the FGM sphere from initial elastic at zero time to third selected time interval for the case $\beta=\varphi=-2$.

www.SID.ir
© 2010 IAU, Arak Branch

Archive of SID

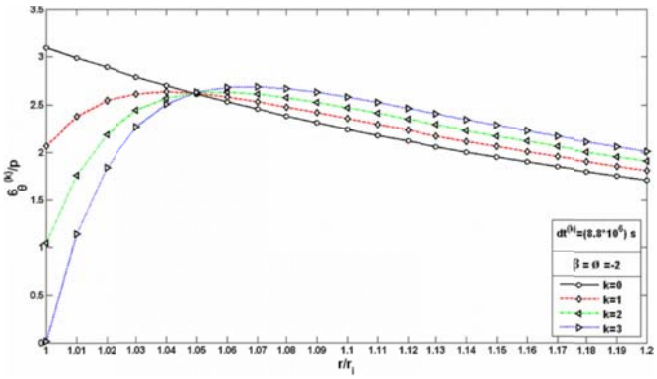

Fig. 16
Time-dependent tangential creep stress redistribution in the FGM sphere from initial elastic at zero time to third selected time interval for the case $\beta=\varphi=-2$.

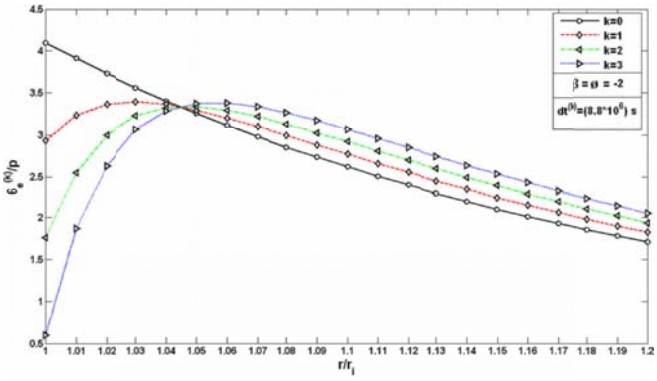

Fig. 17
Time-dependent effective creep stress redistribution in the FGM sphere from initial elastic at zero time to third selected time interval for the case $\beta=\varphi=-2$.

Tangential stress redistribution for this case $\beta=\varphi=2$ is shown in Fig. 7. It is clear that tangential stresses at the inner surface of the vessel are decreasing with time while at the outer surface of the sphere are increasing. Thus, maximum shear stress at the inner surface of the vessel is decreasing with time and at the outer surface of the vessel is increasing with time. This can also be explained by effective stress redistributions shown in Fig. 8. As the effective stress is twice as the maximum shear stress at each point throughout thickness, it is clear that the shear stress distribution becomes more uniform through thickness of the vessel during creep process. Time-dependent stress redistributions for the case $\beta=\varphi=1$ are shown in Figs. 9-11. Stress redistributions take place in the same direction as for the case $\beta=\varphi=2$ but with a higher rate of change with time. Radial, tangential and effective stress redistributions for the materials $\beta=\varphi=-1$ and $\beta=\varphi=-2$ are shown in Figs. 12-17. In Figs. 12 and 15, radial stress redistributions show little changes with time during creep process for both material properties. However, significant changes will occur for tangential and effective stresses with time during creep process as shown in Figs. 13, 14, 16, 17 for both material properties. A reference effective stress can be identified for all cases in which the effective stress is not changing with time during creep process.

4 CONCLUSIONS

Time-dependent creep stress redistribution analysis of thick-walled FGM spheres is investigated for different material properties. Radial stress redistribution is not significant almost for all material properties. But, major redistribution occurs for tangential and effective stresses. The best material is identified by $\beta=\varphi=2$ in which a uniform shear stress distribution will occur throughout the thickness of the FGM sphere. Also minimum changes in stresses with time during creep process belong to this material. A reference effective stress has been identified for all four cases of material properties in which there are no changes in effective stress with time at this point.

www.SID.ir

© 2010 IAU, Arak Branch

Archive of SID

REFERENCES

[1] loghman A., shokouhi N., 2009, Creep damage evaluation of thick-walled spheres using a long-term creep constitutive model, *Journal of Mechanical Science and Technology* **23**: 2577-2582.

[2] Evans R.W., Parker J.D., Wilsher B., 1992, The theta projection concept a model based approach to design and life extention of engineering plant, *International Journal of Pressure Vessels and Piping* **50**: 60-147.

[3] Loghman A., Wahab M.A., 1996, Creep damage simulation of thick-walled tubes using the theta projection concept, *International Journal of Pressure Vessels and Piping* **67**: 105-111.

[4] Sim R.G., Penny R.K., 1971, Plane strain creep behaviour of thick-walled cylinders, *International Journal of Mechanical Sciences* **13**: 987-1009.

[5] Yang Y.Y., 2000, Time-dependent stress analysis in functionally graded material, *International Journal of Solids and Structures* **37**: 7593-7608.

[6] You L.H., Ou H., Zheng Z.Y., 2007, Creep deformation and stresses in thick-walled cylindrical vessels of FGM subjected to internal pressure, *Composite Structures* **78**: 285-291.

[7] Xuan F.-Zh., Chen J.-J., Wang Zh., Tu Sh.-T., 2009, Time-dependent deformation and fracture of multi-material systems at high temperature, *International Journal of Pressure Vessels and Piping* **86**: 604-615.

www.SID.ir
© 2010 IAU, Arak Branch